

Detection of OH and wide HI absorption toward B0218+357

N. Kanekar^{1*}, J. N. Chengalur^{2*}, A. G. de Bruyn^{1,3*}, D. Narasimha^{4*}

¹ Kapteyn Institute, University of Groningen, Post Bag 800, 9700 AV Groningen, The Netherlands

² National Centre for Radio Astrophysics, Post Bag 3, Ganeshkhind, Pune 411 007, India

³ Netherlands Foundation for Research in Astronomy, PO Box 2, 7990 AA Dwingeloo, The Netherlands

⁴ Tata Institute of Fundamental Research, Homi Bhabha Road, Mumbai 400 005, India

Received mmdyy/ accepted mmdyy

ABSTRACT

We present deep GMRT OH and WSRT HI absorption spectra of the $z = 0.6846$ gravitational lens toward B0218+357. Both the 1665 MHz and 1667 MHz OH lines are clearly detected for the first time while a new wide absorption component was detected (at low significance) in the HI spectrum; the OH spectra yielded an OH column density of $N_{\text{OH}} = 2.3 \times 10^{15} \text{ cm}^{-2}$. The ratio of 1667 and 1665 MHz equivalent widths is ~ 1.8 while the redshift of peak OH absorption is $z = 0.68468 \pm 0.000008$ for both lines; this redshift agrees with that obtained from the HI line. The velocity spread (between nulls) of the HI absorption is $\sim 140 \text{ km s}^{-1}$, while that of both OH lines is $\sim 100 \text{ km s}^{-1}$; the HI and OH spectra are broadly similar in that they each have two principal narrow components and a wide absorption trough. We argue that the wide absorption is likely to arise from source components in the Einstein ring and derive a rotation velocity of $\sim 150 \text{ km s}^{-1}$ at a distance of 1.5 kpc from the centre of the $z \sim 0.6846$ galaxy.

Key words: Galaxies: individual: B0218+357 – gravitational lensing – radio lines – ISM

1 INTRODUCTION

Gravitational lensing provides a new probe of the structure of high redshift galaxies through their absorption lines. A typical spiral galaxy at $z \gtrsim 0.5$ is usually too faint for detailed direct observations. However, when such a system gravitationally lenses a distant quasar, forming multiple images of the background source, spectra toward these images allow one to trace the kinematics along several lines of sight through the galaxy. Decimetre wavelength observations of such systems (i.e. spectra in the redshifted HI 21cm and OH radio lines) are particularly well suited to such studies since background sources typically show extended structure at these wavelengths, which allows a better sampling of the velocity field of the intervening galaxy. For example, Chengalur, de Bruyn & Narasimha (1999) used Westerbork Synthesis Radio Telescope redshifted HI and OH spectra of the $z \sim 0.885$ lens toward PKS 1830-211 to estimate the rotation velocity of the absorbing galaxy. The relative strengths of the multiple OH radio lines (when detected) also allow one to trace the large scale distribution of molecular gas in the absorption system. However, the weakness of the OH transitions implies that they have only been detected in three absorbers at cosmological distance (Chengalur et al. 1999; Kanekar & Chengalur 2002).

One of the most well-known (and well-observed !) grav-

itational lenses is the one at $z \sim 0.6846$ toward the source B0218+357 (Patnaik et al. 1993). The radio continuum consists of two images of a flat spectrum source (components A and B), separated by $0.34''$, and a radio ring with a radius of $0.18''$ (Biggs et al. 2001); this is the smallest known Einstein ring. The background source is at a redshift of $z = 0.96$ (Lawrence 1996); the high redshift of the lens and relatively low redshift of the source (with respect to the lens) imply that this system is an excellent candidate to determine the large scale geometry of the Universe and the value of the Hubble constant. In fact, VLA monitoring has yielded a time delay of 10.5 ± 0.4 days between the two images, resulting in a Hubble constant $H_0 = 69^{+13}_{-19} \text{ km s}^{-1} \text{ Mpc}^{-1}$ (Biggs et al. 1999). Unfortunately, however, Hubble Space Telescope (HST) observations have so far not been able to accurately locate the centre of the lens galaxy and this positional uncertainty implies a far higher uncertainty in H_0 than that derived from the statistical errors quoted above (Lehár et al. 2000; Biggs et al. 2001).

The $z = 0.6846$ system has been a rich source of absorption lines, with a number of molecular species such as CO, HCO^+ , HCN, H_2CO and H_2O , as well as HI, already detected here (Wiklind & Combes 1995; Combes & Wiklind 1997; Menten & Reid 1996; Gerin et al. 1997; Carilli, Rupen & Yanny 1993). Further, the difference between the rotation measures of components A and B has been measured to be $\sim 900 \text{ rad m}^{-2}$ and the optical spectrum of B0218+357 is highly reddened (O’Dea et al. 1992; Falco et al. 1999). All of these imply that the lens is an exceedingly gas-rich system; indeed, recent HST obser-

* E-mail: nissim@astro.rug.nl (NK); chengalu@ncra.tifr.res.in (JNC); ger@nfra.nl (AGdB); dna@astro.tifr.res.in (DNA)

vations (Lehár et al. 2000) have shown that the system is a late-type spiral galaxy.

The original observations of the HI absorption profile (Carilli et al. 1993) were of low sensitivity and spectral resolution and hence could not resolve out the absorption feature. Further, the full width between nulls of the HI profile was measured to be 75 km s^{-1} , somewhat small for a spiral galaxy at a moderate inclination, especially given the extended structure of the background continuum. We present here deep Giant Metrewave Radio Telescope (GMRT) OH and Westerbork Synthesis Radio Telescope (WSRT) HI observations of the $z = 0.6846$ system; both the 1665 MHz and 1667 MHz OH lines were detected while strong limits were placed on the optical depth of the 1720 MHz OH transition. We also detect a wide component to the HI absorption, with a velocity spread of $\sim 140 \text{ km s}^{-1}$. The observations and data analysis are discussed in section 2 while the implications for the $z = 0.6846$ absorber are discussed in section 3.

2 OBSERVATIONS AND DATA ANALYSIS

2.1 WSRT HI observations

Observations of the redshifted HI line toward B0218+357 were carried out with the WSRT on 21 June 1998, with the new DZB correlator as the backend. A bandwidth of 2.5 MHz was used for the observations, centered at an observing frequency of 843.20 MHz and sub-divided into 256 channels. No taper was applied in the lag-to-frequency transform, yielding a velocity resolution of $\sim 3.5 \text{ km s}^{-1}$ (channel resolution $\sim 9.8 \text{ kHz}$). 12 telescopes were used for the observations.

The standard calibrators 3C48 (30min, before) and 3C286 (72min, after), were used to calibrate the absolute flux scale and the system bandpass; their adopted flux densities are on the Baars et al. (1977) scale. The total on-source time was 11.7 hours.

2.2 GMRT OH observations

The GMRT OH observations of B0218+357 were initially carried out on the 17th and 27th of June, 2001, with the standard 30 station FX correlator as the backend. A total bandwidth of 4 MHz was used for these observations, to include both the main OH transitions (at rest frequencies of 1665.4018 MHz and 1667.3590 MHz). This was sub-divided into 128 channels, yielding a frequency resolution of $\sim 31.25 \text{ kHz}$ (i.e. $\sim 9.4 \text{ km s}^{-1}$) on each run. Twenty three and seventeen antennas were available for the observations on the 17th and the 27th respectively, due to various debugging and maintenance activities. The standard calibrator 3C48 was used to carry out absolute flux and bandpass calibration. Total on-source times were 3 and 5 hours on the first and second observing dates respectively.

While the 4 MHz bandwidth observations were important for the initial detection of the OH lines, it was apparent that their relatively poor velocity resolution would not allow the positions or widths of the absorption features to be determined as accurately as in the case of the HI line (note that the GMRT correlator allows a higher frequency resolution only at the cost of total bandwidth and the bandwidth of 4 MHz was necessary to include both OH features in the band). Further observations (each using a bandwidth of 1 MHz, i.e. a resolution of $\sim 7.8 \text{ kHz}$ or $\sim 2.4 \text{ km s}^{-1}$) were hence separately carried out of the 1665 MHz and 1667 MHz features, on the 11th of October and the 27th of November, 2001, respectively.

21 antennas were available for each of these observations; the total on-source times were ~ 6 hours and ~ 3 hours for the 1665 MHz and 1667 MHz observations respectively. Absolute flux and bandpass calibration were carried out using 3C48 and 3C147.

Finally, an attempt was also made with the GMRT to detect the 1720 MHz OH transition in the $z \sim 0.6846$ absorber. These observations were carried out on the 25th of November, 2001, using a bandwidth of 1 MHz (i.e. a resolution of $\sim 7.8 \text{ kHz}$ or $\sim 2.3 \text{ km s}^{-1}$). Flux and bandpass calibration were again carried out using 3C48 and 3C147. The total on-source time was ~ 3 hours, with 28 antennas.

2.3 Data analysis and spectra

The data were converted from the telescope format to FITS in all cases and then analyzed in AIPS using standard procedures. A careful inspection was initially carried out for RFI and sections showing evidence of interference were flagged out. For the WSRT data, a simple average of the visibilities was made after bandpass calibration and the peak flux density read off from the image cube; this resulted in the spectrum shown in figure 1. We note that B0218+357 is largely unresolved on WSRT baselines; the spectrum represents the flux density averaged over 60 interferometers. A total of 6 baselines were not used in the averaging for various reasons. In the case of the GMRT observations, after phase and bandpass calibration, the continuum emission was subtracted by fitting a linear polynomial to the U-V visibilities, using the AIPS task UVLIN. The continuum-subtracted data were then mapped in all channels and spectra extracted at the quasar location from the resulting three-dimensional data cube. In the case of the multi-epoch 4 MHz GMRT observations, the spectra of the two epochs were corrected to the heliocentric frame outside AIPS and then averaged together.

The flux density of B0218+357 was measured to be 1.520 Jy (at 843 MHz) in the WSRT observations. In the case of the GMRT observations, the flux density was measured to be 1.64 Jy (17th and 27th of June), 1.54 Jy (11th of October) and 1.58 Jy (27th of November) at $\sim 989 \text{ MHz}$ and 1.66 Jy at $\sim 1021 \text{ MHz}$ (25th of November). Note that all spectra of the 1665 MHz and 1667 MHz lines have been scaled here to a common flux density of 1.64 Jy. Earlier experience with the GMRT indicates that the flux calibration is reliable to $\sim 15\%$, in this observing mode.

The WSRT HI spectrum is shown in figure 1[A]; the spectrum has been Hanning smoothed and re-sampled and has a velocity resolution of $\sim 7 \text{ km s}^{-1}$ and an RMS noise of $\sim 7 \text{ mJy}$. Two deep features can be immediately identified in the spectrum, besides a weak broad component. The peak optical depth is 0.05, occurring at a redshift of 0.68467 ± 0.00001 . The total velocity spread of the absorption is $\sim 150 \text{ km s}^{-1}$. The spectrum has a total velocity coverage of $\sim 800 \text{ km s}^{-1}$; only the central 400 km s^{-1} are shown here, for comparison with the high resolution OH spectra. We note that non-Gaussian behavior was observed at two locations in the spectrum, near the edges of the band (beyond the velocity range plotted in figure 1 [A]); these are likely to be due to low-level RFI.

The final GMRT 4 MHz OH spectrum toward B0218+357 is shown in figure 2. The RMS noise is 1.1 mJy, per 9.4 km s^{-1} channel; the spectrum has not been smoothed. Both OH transitions are clearly visible; the peak absorption occurs at heliocentric frequencies of 988.56 MHz and 989.72 MHz, both implying a redshift $z = 0.68468 \pm 0.00003$. A wide shoulder can be seen in both absorption features, on the high frequency side of the principal feature.

Figures 1[B] and 1[C] show the 1 MHz bandwidth GMRT

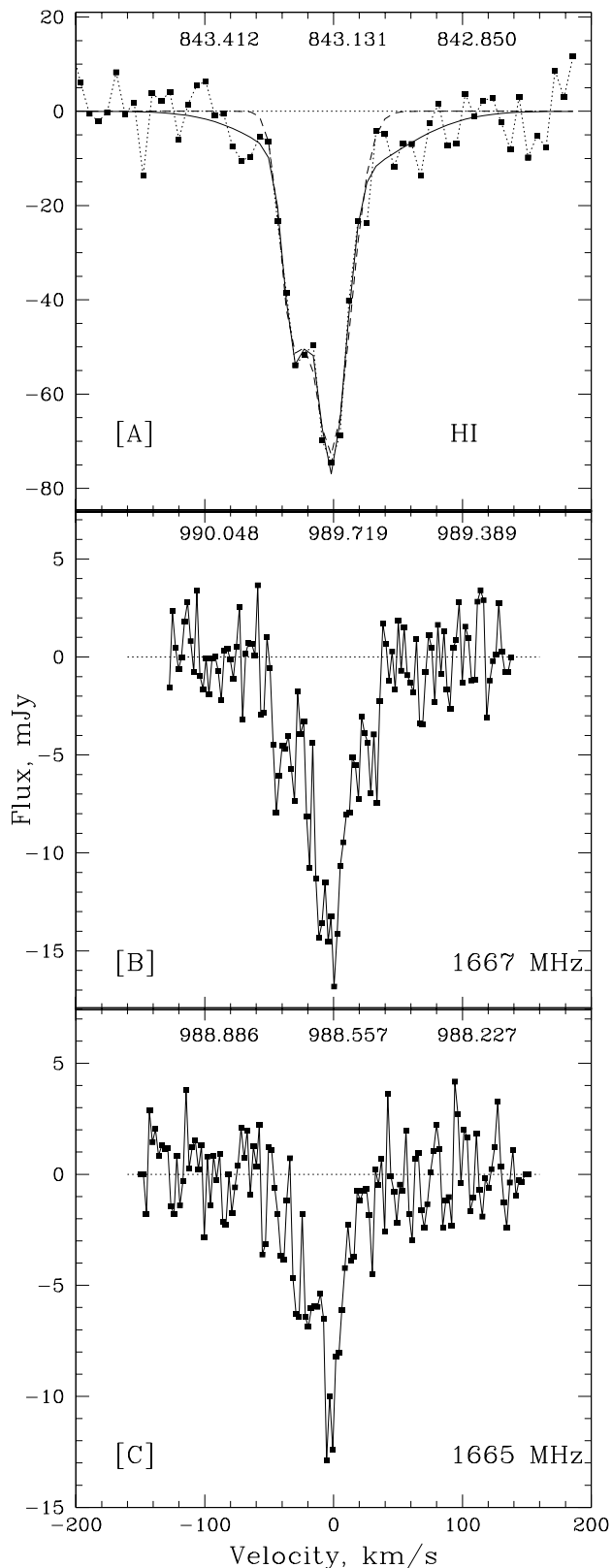


Figure 1. Absorption spectra toward B0218+357 : [A] WSRT 7 km s^{-1} resolution HI spectrum (solid squares); the solid line shows the 3-Gaussian fit. [B] GMRT 2.4 km s^{-1} resolution spectrum in the 1667 MHz OH line and [C] GMRT 2.4 km s^{-1} resolution spectrum in the 1665 MHz OH line. The x-axis of each panel is velocity, in km/s, relative to $z = 0.68468$; the heliocentric frequency scale (in MHz) for each line is at the top of each panel.

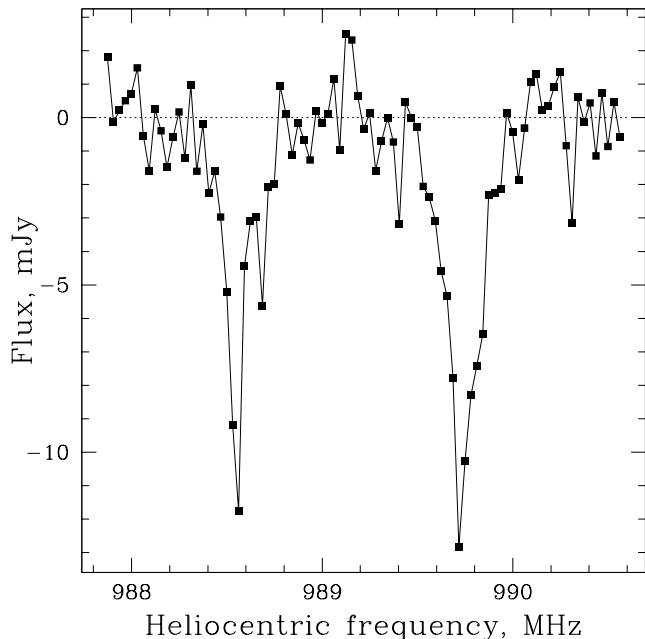


Figure 2. GMRT 9.4 km s^{-1} resolution OH spectrum toward B0218+357. The 1665 MHz and 1667 MHz OH lines can be clearly seen.

spectra of the 1667 MHz and 1665 MHz OH lines. The RMS noise values are 1.5 mJy and 1.6 mJy respectively, per 2.4 km s^{-1} channel (the spectra have again not been smoothed). The high frequency shoulder of the 4 MHz spectrum is now resolved out in both spectra; besides this, a wide absorption component can also be seen (which is stronger in the 1667 MHz transition). The equivalent width of the 1667 MHz absorption line is $\int \tau_{1667} dV = 0.40 \pm 0.01 \text{ km s}^{-1}$, while the ratio of the 1667 MHz and 1665 MHz equivalent widths is $R \sim 1.8$, as expected in optically thin conditions in thermal equilibrium. Interestingly, this ratio is slightly larger at the low frequency edge of the two profiles (at $\sim 20 \text{ km s}^{-1}$). The total velocity spread of both the 1665 and 1667 MHz lines is $\sim 100 \text{ km s}^{-1}$.

The peak optical depth in the 1 MHz bandwidth spectra occurs at heliocentric frequencies of 988.575 MHz (1665 MHz transition) and 989.717 MHz (1667 MHz transition), corresponding to redshifts 0.68465 ± 0.000008 and 0.68468 ± 0.000008 respectively. While the above redshifts are in marginal disagreement, figure 1[C] shows that the 1665 MHz line has two peaks of approximately the same depth, separated by $\sim 7.2 \text{ km s}^{-1}$. If the second (marginally weaker) feature is used to compute the redshift, one obtains $z_{1665} = 0.68468$, in agreement with the 1667 MHz redshift; the same value is also obtained by a Gaussian fit to the 1665 MHz line. We will hence use this value for the redshift of the absorber, as it also agrees with that estimated from the 1667 MHz line. This is also in broad agreement with redshifts obtained from millimetre-wave transitions (e.g., $z = 0.684693$, from the ^{13}CO line; Wiklind & Combes 1997). Note that a measured difference between the redshifts of the four OH 18cm lines can, in principle, be used to simultaneously measure variations in the fine structure constant α , the ratio of electron mass to proton mass m_e/m_p and the proton g-factor g_p (Chengalur & Kanekar 2003).

Finally, the GMRT spectrum of the 1720 MHz OH transition (not shown here) did not show any absorption. The RMS noise was measured to be 1 mJy , after smoothing the spectrum to a resolution

of $\sim 10 \text{ km s}^{-1}$; this yields a 3σ limit of 0.0018 on the optical depth in the 1720 MHz line, per 10 km s^{-1} .

3 DISCUSSION

The OH and HI profiles are broadly similar in that each absorption line consists of a primary component, a high frequency shoulder and a broad shallow trough; this indicates that the lines originate in the same diffuse or dark cloud. While the total width of the HI absorption is wider than that of the OH lines ($\sim 150 \text{ km s}^{-1}$ for the HI absorption against $\sim 100 \text{ km s}^{-1}$ for the OH), this is not too surprising since OH is believed to be more confined than HI in models of molecular clouds (see, for example, figure 6 in Liszt & Lucas 1996). It is tempting to identify the two main features of the lines as stemming from absorption against the two point images A and B; however, VLBI observations of the HI absorption (Carilli et al. 2000) have shown that it arises solely due to image A, while no absorption is seen against image B. Similarly, the mm-wavelength molecular absorption lines are also only seen against image A and not against B (Menten & Reid 1996). The two main features of the lines hence probably arise from the two VLBI components of image A (Patnaik et al. 2003, in preparation) or possibly from multiple clouds along the line of sight to one of these components, while the broad but shallow trough is likely to stem from absorption against source components in the radio ring.

For an optically thin cloud in thermal equilibrium, the OH column density of the absorbing gas N_{OH} is related to the excitation temperature T_x and the 1667 MHz optical depth τ_{1667} by the expression (e.g. Liszt & Lucas 1996)

$$N_{\text{OH}} = 2.24 \times 10^{14} \left(\frac{T_x}{f} \right) \int \tau_{1667} dV, \quad (1)$$

where f is the covering factor of the absorber. Here, N_{OH} is in cm^{-2} , T_x in K and dV in km s^{-1} . The integrated optical depth in the 1667 MHz line is $\int \tau_{1667} dV = 0.659 \text{ km s}^{-1}$; thus, $N_{\text{OH}} = 1.1 \times 10^{14} \times (T_x/f) \text{ cm}^{-2}$. VLBI observations (Carilli et al. 2000) have shown that no HI absorption is seen against component B; similarly, the CO and HCO^+ absorption are only seen against component A (Wiklind & Combes 1995); the covering factor f is thus likely to be close to 0.4. Next, the OH excitation temperature T_x cannot be directly estimated for cosmologically distant objects such as the $z \sim 0.6846$ absorber. In the Galaxy, OH emission studies have shown that this temperature may be as low as $T_x \sim T_{\text{CMB}} + 1 \text{ K}$, with similar values for the HCO^+ line ($T_x(\text{HCO}^+) \sim T_{\text{CMB}}$; Lucas & Liszt 1996). However, the excitation temperatures of the redshifted HCO^+ lines in the four known high redshift absorbers have been found to be higher than $T_{\text{CMB}}(1+z)$, the redshifted CMB temperature; it is thus quite likely that the OH excitation temperature too is higher in these systems. Given that the $z = 0.6846$ absorption system is believed to originate in a late-type spiral disk (Lehár et al. 2000), we will, in the absence of additional information, assume $T_x = 10 \text{ K}$, a typical temperature in dark clouds in the Milky Way, to estimate the OH column density. This yields $N_{\text{OH}} = 2.3 \pm 0.06 \times 10^{15} (T_x/10)(0.4/f) \text{ cm}^{-2}$; note that this is slightly different from the value $N_{\text{OH}} = 2.65 \times 10^{15} (T_x/10)(0.4/f) \text{ cm}^{-2}$, obtained by Kanekar & Chengalur (2002) from the lower resolution ($\sim 9.4 \text{ km s}^{-1}$) spectrum. The present value is obtained from the 1 MHz bandwidth, $\sim 2.4 \text{ km s}^{-1}$ resolution spectrum.

The OH column density of the absorber can be used to estimate the HCO^+ and H_2 column densities, by the relations

Table 1. Three-component Gaussian fit to the HI absorption

Component	1	2	3
Frequency (MHz)	843.136	843.216	843.126
Redshift,	0.684669(5)	0.684510(7)	0.68469(4)
Line flux (mJy)	63.3 ± 6.6	39.6 ± 6.3	13.5 ± 5.6
FWHM (km s^{-1})	26.6 ± 4.2	19.8 ± 4.6	115 ± 30

$N_{\text{HCO}^+} \approx 0.03 \times N_{\text{OH}}$ and $N_{\text{H}_2} \approx 1 \times 10^7 \times N_{\text{OH}}$ (Liszt & Lucas 1999; see also Kanekar & Chengalur 2002). This yields $N_{\text{HCO}^+} = 6.8 \times 10^{13} \text{ cm}^{-2}$, in good agreement with that measured from the HCO^+ line ($N_{\text{HCO}^+} = 7.4 \times 10^{13} \text{ cm}^{-2}$; Wiklind & Combes 1995). We also obtain $N_{\text{H}_2} = 2.3 \times 10^{22}$, which is, interestingly enough, in excellent agreement with the value of Gerin et al. (1997) ($N_{\text{H}_2} = 2 \times 10^{22} \text{ cm}^{-2}$), using the ^{17}CO line, but a factor of 20 smaller than the estimate of $N_{\text{H}_2} = 5 \times 10^{23} \text{ cm}^{-2}$, from the CO absorption (Wiklind & Combes 1995).

We next attempt to decompose the HI absorption into its components by simultaneously fitting Gaussians to the three main absorption features; we do not fit to the OH profiles as the signal-to-noise ratio of the wide component in the high resolution OH spectra is too low to get a stable fit. While it is quite unlikely that the net result of absorption against the components of the ring is indeed a Gaussian, the decomposition will be used solely to quantify the velocity spread of the absorption profile, in order to estimate the rotation velocity of the absorbing galaxy. We note that the results do not change significantly if we assume that the broad feature has a ‘‘Top-hat’’-like shape (while retaining a Gaussian shape for the two deep components).

Figure 1[A] shows the 3-Gaussian fit to the Hanning smoothed HI absorption profile; here, the Hanning smoothed (and re-sampled) 7 km s^{-1} resolution spectrum is plotted as solid squares while the 3-Gaussian fit is shown as a solid line. Attempts were also made to fit only two Gaussians to the profile. The dashed line in fig. 1[A] shows the best 2-Gaussian fit; this fails to reproduce the wide absorption trough on either side of the two main components. Two-component fits were thus found to leave clear residuals, indicating that a 3-component fit was indeed necessary. The parameters of the 3-Gaussian fit are listed in Table 1; it should be pointed out that the fit to the broad absorption has only a weak ($\sim 2.4\sigma$) significance. Deeper HI observations would be useful to test the reality of this feature, which would be very interesting if it were shown to indeed arise against the radio ring. Since the ring is only prominent at low frequencies (it is almost undetectable at 22 GHz but has more flux than Image B in the 1.67 GHz EVN observations of Patnaik et al. 2003), deeper HI observations would provide the best sampling of the large scale kinematics of the lens galaxy. Finally, the FWHM of the broad absorption component is $115 \pm 30 \text{ km s}^{-1}$; more relevant, the spread between points on the spectrum at which this component falls below the 1σ level is $\sim 140 \text{ km s}^{-1}$. This gives the total spread of the absorption against the radio ring.

The 5 GHz VLBI image of Patnaik et al. (1993) (see also Biggs et al. 2001) shows that image B lies roughly at the centre of the ring while the two components of image A lie outside the ring, at a distance of $\sim 200 \text{ mas}$. The fact that the narrow absorption features due to the components of image A lie quite close to the centre

of the broad absorption trough implies that these components lie close to the kinematic minor axis of the absorbing galaxy; it is thus difficult to draw strong conclusions about the rotation curve of the galaxy from these absorption lines. The observed lack of absorption against component B makes it likely there is a “hole” in the HI distribution near the centre of the $z = 0.6846$ absorber, similar to the situation in the Milky Way and other local spirals. As mentioned above, the wide HI absorption is likely to stem from absorption toward source components in the Einstein ring. This implies that the line-of-sight rotation velocity at $0.18''$ from the lens centre (i.e. at the location of the source components in the ring) is approximately 70 km s^{-1} . Since the lens is at an inclination of around 25 degrees, the rotation velocity is $\sim 150 \text{ km s}^{-1}$, fairly reasonable for an ordinary spiral galaxy.

In conclusion, we have detected both the 1665 MHz and 1667 MHz OH transitions in absorption in the $z = 0.68468$ gravitational lens toward B0218+357 and have also found a wide absorption component in the HI profile (at low significance). The redshifts of peak OH absorption are in good agreement with that of the HI, as well as with those of molecular lines discovered earlier in the absorber. The HI absorption is spread over 140 km s^{-1} while both OH lines have a velocity spread of $\sim 100 \text{ km s}^{-1}$. The OH column density of the absorber is $N_{\text{OH}} = 2.3 \times 10^{15} (T_x/10)(0.4/f) \text{ cm}^{-2}$. Finally, we estimate that the rotation velocity of the galaxy is $\sim 150 \text{ km s}^{-1}$, at around 1.5 kpc from the centre.

Acknowledgments

We thank the staff of the GMRT that made these observations possible. GMRT is run by the National Centre for Radio Astrophysics of the Tata Institute of Fundamental Research. The Westerbork Synthesis Radio Telescope is operated by the ASTRON (Netherlands Foundation for Research in Astronomy) with support from the Netherlands Foundation for Scientific Research (NWO).

REFERENCES

- Baars J. W. M., Genzel R., Pauliny-Toth I. I. K., Witzel A., 1977, *A&A*, 61, 99
- Biggs A. D., Browne I. W. A., Helbig P., Koopmans L. V. E., Wilkinson P. N., Perley R. A., 1999, *MNRAS* 304, 349
- Biggs A. D., Browne I. W. A., Muxlow T. W. B., Wilkinson P. N., 2001, *MNRAS* 322, 831
- Carilli C. L., Rupen M. P., Yanny B., 1993, *ApJ* 412, L59
- Carilli C. L. et al., 2000, *Phys. Rev. Lett.*, 85, 2511
- Chengalur J. N., de Bruyn A. G., Narasimha D., 1999, *A&A* 343, L79
- Chengalur J. N., Kanekar, N., 2003, *Phys. Rev. Lett.*, accepted
- Combes F., Wiklind T., 1997, *ApJ* 486, L79
- Falco E. et al. 1999, *ApJ* 523, 617
- Gerin M., Phillips T. G., Benford D. J., Young K. H., Menten K. M., Frye B., 1997, *ApJ* 488, L31
- Kanekar N., Chengalur J. N., 2002, *A&A* 381, L73
- Lehár J. et al., 2000, *ApJ* 536, 584
- Liszt H., Lucas R., 1996, *A&A* 314, 917
- Lucas R., Liszt H., 1996, *A&A* 307, 237
- Liszt H., Lucas R., 1999, in *ASP Conf. Ser. 156, Highly Redshifted Radio Lines*, C. L. Carilli et al. eds., 188
- Lawrence C. L., 1996, *IAU Symp. 173, Astrophysical Applications of Gravitational Lensing*, eds. C. S. Kochanek & J. N. Hewitt (Dordrecht:Kluwer), 299
- Menten K. M., Reid M. J., 1996, *ApJ* 465, L99
- O’Dea C. et al., 1992, *AJ*, 104, 1320
- Patnaik A. R., Browne I. W. A., King L. J., Muxlow T. W. B., Walsh D., Wilkinson P. N., 1993, *MNRAS* 261, 435
- Wiklind T., Combes F., 1995, *A&A* 299, 382
- Wiklind T., Combes F., 1997, *A&A* 328, 48